A LIMIT ON THE LARGE ANGULAR SCALE POLARIZATION OF THE COSMIC MICROWAVE BACKGROUND

Brian G. Keating[1], Christopher W. O'Dell, Angelica de Oliveira-Costa[2], Slade Klawikowski, Nate Stebor[3], Lucio Piccirillo[4], Max Tegmark[2], and Peter T. Timbie
Department of Physics, University of Wisconsin – Madison, Madison, WI 53706
Draft version July 3, 2001

ABSTRACT

We present an upper limit on the polarization of the Cosmic Microwave Background at 7° angular scales in the frequency band between 26 and 36 GHz, produced by the Polar experiment. The campaign produced a map of linear polarization over the R.A. range $112° - 275°$ at declination 43°. The model-independent upper limit on the E-mode polarization component of the CMB at angular scales $\ell = 2 - 20$ is 10μK (95% confidence). The corresponding limit for the B-mode is also 10μK. Constraining the B-mode power to be zero, the 95% confidence limit on E-mode power alone is 8μK.

Subject headings: cosmic microwave background: – cosmology: observations – polarization

1. INTRODUCTION

The Cosmic Microwave Background (CMB) is completely specified by three characteristics: its spectrum, the spatial distribution of its total intensity, and the spatial distribution of its polarization. In the past decade, measurements of its spectrum and temperature anisotropy have ushered in an era of precise determinations of numerous cosmological parameters. CMB polarization has the potential to provide powerful cross-checks as well as to improve the accuracy with which cosmological parameters can be measured, most strikingly those related to gravitational waves and the ionization history of the Universe. Both of these phenomena imprint a signature on the polarization of the CMB at the largest angular scales $\ell \lesssim 30$. We have built a polarimeter called Polarization Observations of Large Angular Regions (Polar) which is optimized to study CMB polarization at these scales.

The polarization of the CMB is a unique probe of radiative transport in the pre-galactic plasma. Thomson scattering of anisotropic CMB radiation by free electrons produces CMB polarization, which therefore carries information about the Universe during the periods when it was ionized. Information about the early ($z \lesssim 1000$) ionized epoch is encoded in degree-scale polarized fluctuations, whereas information about reionization is imprinted on scales of tens of degrees, corresponding to the horizon scale at the time. Therefore, CMB polarization provides the crucial evolutionary link from the recombination epoch ($z \sim 1000$) to the period of large scale structure formation ($z \sim 6$). In particular, reionization should produce a new polarized peak near $\ell \lesssim 20$, the peak location depending on the redshift z_i at which the first luminous objects heated and reionized the Universe (Zaldarriaga 1998; Keating et al. 1998). Despite its fundamental importance, z_i is still quite poorly constrained observationally: the lack of an observed Lyman-α trough (due to neutral hydrogen) in the spectra of distant quasars (Gunn & Peterson 1965) places a lower limit $z_i \gtrsim 6$, whereas the lack of observed suppression of the unpolarized acoustic peaks gives an upper limit $z_i \lesssim 20$ (Wang, Tegmark, & Zaldarriaga 2001). The purpose of this *Letter* is to present the strongest limits to date on CMB polarization on the angular scales $\ell \lesssim 30$ relevant to these polarized peaks.

[1] Current Address: Department of Physics, California Institute of Technology, Pasadena, CA 91125; bgk@astro.caltech.edu.

[2] Department of Physics, University of Pennsylvania, Philadelphia, PA 19104

[3] Department of Physics, University of California at Santa Barbara, Santa Barbara, CA 93106

[4] Department of Physics and Astronomy, University of Wales - Cardiff, Wales, UK CF24 3YB

2. INSTRUMENT

Polar's design builds on techniques developed in previous searches for CMB polarization (Nanos 1979; Lubin & Smoot 1980; Wollack et al. 1993) and is driven by the magnitude and angular scale of the anticipated CMB signal, and rejection of potential systematic effects. The polarimeter is a superheterodyne correlation radiometer which detects two orthogonal linear polarization states in three radiofrequency (RF) bands in the K_a-band between 26-36 GHz. The two polarization states $i \in \{x, y\}$, $E_i^{RF}(t, \nu, \phi_i) = E_i \cos(2\pi\nu t + \phi_i)$ enter a single-mode corrugated feedhorn and are separated by an orthomode transducer (OMT). The OMT's high polarization isolation (> 30 dB) ensures low cross-polarization. E_i^{RF} are amplified by separate HEMT amplifiers (Pospieszalski 1992) cooled to 25 K by a mechanical cryocooler. Downconversion from the RF band to an intermediate frequency (IF) band (2-12 GHz) is performed by Schottky diode mixers, driven by a Gunn diode local oscillator (LO) at 38 GHz. In the IF band the two polarization states are amplified producing $E_i^{IF} \propto E_i^{RF}$, and filtered into three separate IF bands, denoted J1, J2, and J3. The IF bands translate into RF bands: J1 (32-36 GHz), J2 (29-32 GHz), and J3 (26-29 GHz). Prior to filtering, two diode detectors measure the total power of each polarization state, which monitors atmospheric opacity. E_x^{IF} and E_y^{IF} are correlated by three Schottky Diode analog multiplier circuits. The phase of the LO is switched between 0 and π at 1 KHz prior to mixing the E_y^{RF} waveform. The voltage produced by the correlators at this stage thus switches between $\kappa E_x^{RF} E_y^{RF}$ and $-\kappa E_x^{RF} E_y^{RF}$ at 1 KHz, where κ is the intensity-to-voltage conversion factor. Phase-sensitive detection of this modulated signal reduces the effects of low frequency drifts in the HEMTs and subsequent components to negligible levels. After low-pass filtering, we

record an audio-band signal with a DC component $I_{DC} = \kappa\langle E_x^{RF} E_y^{RF}\rangle$, where the brackets denote a time-average, and AC components proportional to the thermal noise from the radiometer, atmosphere, and celestial signals. These signals are referred to as the "science channels". A second lock-in amplifier for each correlator is referenced to the same 1 KHz waveform but delayed in phase by $\pi/2$ with respect to the phase switch. These signals, hereafter referred to as "quadrature phase channels" (QPC), contain only the noise terms of the RF band and no optical or celestial signals. The QPC are powerful probes of systematic effects produced solely by the radiometer and post-detection stages. The output from the QPC is proportional to the noise equivalent temperature (NET) of the instrument. For a correlation radiometer this is $\mathrm{NET} = \sqrt{2/\Delta\nu}(\mathrm{T_{Rx}} + \mathrm{T_{Ant}})[\mathrm{K - s^{1/2}}]$, where $\Delta\nu$ is the bandwidth of the radiometer, $T_{\rm Rx}$ is the receiver noise temperature, and $T_{\rm Ant}$ is the antenna temperature of observed optical sources, including diffuse sources such as the atmosphere and the CMB itself. A schematic outline of POLAR is presented in Keating et al. (1998), and Keating (2000) presents the complete design. The specifications of POLAR are summarized in Table 1.

Absolute calibration of the polarimeter is accomplished by placing a 0.003" polypropylene sheet in the near-field of the antenna, tilted at an angle of 45° relative to the optical axis. The dielectric sheet introduces a polarized signal into the antenna due to the difference in reflection between the parallel and perpendicular electric fields. We calibrate the polarimeter by rotating it around the optical axis. Near-field, absolute calibration of previous CMB polarimeters have used wire-grids to reflect the fields parallel to the wire axes (Lubin & Smoot 1980). The dielectric sheet material and thickness are chosen to produce an absolute polarized antenna temperature of ~ 500 mK versus 200 K for wire-grid calibrators. This provides a calibration reference near the NET of the radiometer (accurate to 10%), which reduces the dynamic range requirements on the IF and post-detection stages. A χ^2 minimization fit to a radiometer model is computed during calibration, which determines not only the radiometer flux scale, but also inter-channel cross-talk and gain imbalance between the two polarization states (Keating 2000).

TABLE 1
POLAR INSTRUMENT SPECIFICATIONS

Channel[a]	ν_c[b] [GHz]	$\Delta\nu$[c] [GHz]	FWHM[d] [°]	$\overline{T_{\rm pol}}$[e] [μK]	$S_{\rm sky}$[f] [mK − s$^{1/2}$]
TP-E/H	31.9	7.8/8.0	7.0	···	14.0/20.0
J3	27.5	0.8	7.7	84(28)	1.9
J2	30.5	2.0	7.4	72(14)	1.0
J1	34.0	1.9	7.1	33(11)	1.0

[a]TP-E and TP-H measure the total power in the E and H polarization planes of the Horn/OMT assembly prior to correlation.

[b]Channel Band Centroid

[c]Channel Bandwidth.

[d]E and H-plane Beamwidths are equal to within 5%. Measured feed/OMT cross-polarization is < -40dB for all channels.

[e]Mean Polarized Offset $\overline{T_{\rm pol}} = \sqrt{\overline{Q}^2 + \overline{U}^2}$, where $\overline{Q}$ and $\overline{U}$ are the Stokes parameter offsets. Numbers in parentheses denote the corresponding values for the QPC.

[f]Measured channel NET for a typical clear day with $K_{\rm a}$-band zenith sky temperature $T_{Atm} \simeq 15$ K. NET measured at Stokes modulation frequency 0.065 Hz.

3. OBSERVATIONS

The POLAR campaign collected a total of 746 hours of data between 2000 March 11 and 2000 May 29. Both Stokes parameters Q and U were observed through the same atmospheric column by a single corrugated scalar feedhorn cooled to $\sim$ 40K. The feed produces a nearly frequency independent beam with a FWHM $\simeq 7.0°$. The beam observes the zenith from Madison, Wisconsin, which corresponds to a declination of $\delta = 43°01'48''$. Contamination by terrestrial radiation is minimized by our choice of vertical drift scans and is further mitigated by two levels of ground shields (one co-rotating with the polarimeter, and the other fixed relative to the ground). Thus, radiation from the ground must diffract over two ground screens before reaching the antenna.

The Stokes parameters completely describe the linear polarization state of radiation produced by Thomson scattering (Chandrasekhar 1960; Hu & White 1997) and are modulated by rotation of the entire instrument around its optical axis. The radiometer rotates at $f = 0.033$Hz. The Stokes parameters are modulated at $2f$ whereas most potential systematic signals are modulated at f or DC, and are easily discriminated from Q and U. Measurement of both Q and U is essential for model independent recovery of the 'Electric' (or 'Gradient') and 'Magnetic' (or 'Curl') components of the polarization power spectrum (Zaldarriaga & Seljak 1997; Kamionkowski, Kosowsky, & Stebbins 1997).

4. DATA REDUCTION AND MAPS

The data were sampled at 20 Hz and converted from digital units to Stokes Q and U for each 7.5 minute file. Each file contains ~ 14 rotations of the polarimeter during which the beam moves $\sim 1.9°$. For each file, the data are sorted into discrete angular bins and synchronously demodulated with respect to trigonometric functions of the rotation angle. In our coordinate system, defined with respect to the local geographic coordinates, we perform a χ^2 minimization of the angular binned data fit to the function

$$I(\theta_t) = I_o + C\cos\theta_t + S\sin\theta_t + Q\cos 2\theta_t + U\sin 2\theta_t, \quad (1)$$

where $\theta_t = 2\pi f t$. In addition to the Stokes parameters Q and U, the terms C and S (which are synchronous with the rotation at frequency f) are monitored to determine our sensitivity to rotation-synchronous systematic effects, and to monitor atmospheric fluctuations.

Three levels of diagnostics were used to detect and remove contaminated data: 1) housekeeping and weather (dewpoint, cloud cover) cuts; 2) time ordered data (TOD) cuts; 3) rotation ordered data (ROD) cuts after constructing the Stokes parameters. Data were collected while the

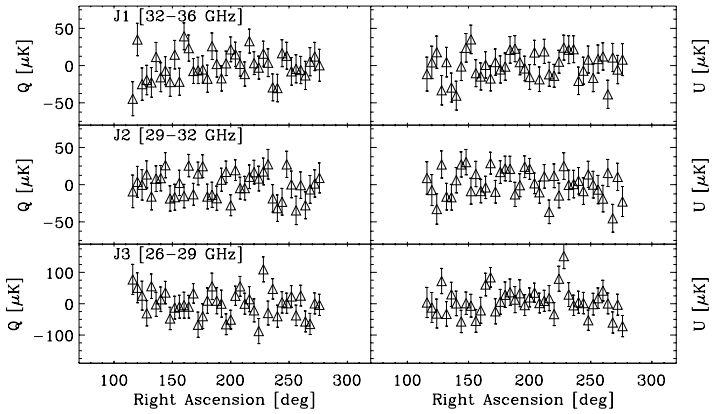

FIG. 1.— Maps of the Stokes parameters vs. R.A. for each frequency channel in thermodynamic temperature. For display purposes, the maps are binned into 4° R.A. pixels with Galactic latitude $|b| > 25°$, though the analysis uses 2° pixels. The sky coverage was determined by our scan strategy and data selection criteria. The Stokes parameters are presented in accordance with the IAU definition.

sun (moon) was less than 30° (60°) above the horizon. Approximately 2% of the total data collected were removed due to work on the receiver or closure of the observatory dome. 1.5% of the data were removed due to completely overcast cloud cover. Although atmospheric emission is not expected to have significant linear polarization at 30 GHz (Keating et al. 1998), the correlators are sensitive to changes in the total antenna temperature. This coupling is caused by imperfect isolation between the E and H planes of the OMT and results in a weak dependence of the correlators on their total bias power (Carretti et al. 2001). The bias power is proportional to the system temperature, including atmospheric emission. Since the atmospheric fluctuation spectrum at 30 GHz falls approximately as $1/f^{\alpha}$ ($\alpha \geq 1$), due to fluctuations in the amount of precipitable water vapor, there is residual power at the Stokes parameter modulation frequency 0.065 Hz. This effect is correlated between all frequency channels, and produces a slow drift in the demodulated Stokes parameters, as well as in the rotation synchronous terms S and C in equation 1. We require that the rotation synchronous terms S and C be less than 2×NET. This cut (applied after the TOD has been assembled into the ROD) removes almost all weather-related contamination of the science channels (35% of the total data). Since the basis functions for S and C are orthogonal to those of Q and U, we are assured that only data collected during poor weather, and not polarized celestial signals, are flagged. Further data files (2.6%) are removed if any samples in the file deviate more than 5σ from the TOD-mean, or 3σ from ROD-mean. After application of all cuts, 121 hours (16%) of the total collected data survive. The science channels display mean inter-channel cross-correlation coefficients of 1% in the TOD, primarily caused by correlated atmospheric fluctuations or HEMT gain fluctuations (Wollack & Pospieszalski 1998). The QPC display similar correlations. Correlations between Stokes parameters in the ROD average 10%, for the science channels and ∼ 3% for the QPC. For each section of data that passes the data quality tests, the time-ordered data are converted to a map and covariance matrix via the minimum variance map-making procedure outlined in Tegmark (1997). The 25 total sections range in length from 4-24 hours. An overall offset is removed from each section, and the data covariance matrix is adjusted accordingly (Tegmark 1997; Bond, Jaffe, & Knox 1998). All sections are combined into a final map and covariance matrix for each channel. Figure 1 presents the maps of the Stokes parameters for all correlator channels versus RA.

5. FOREGROUNDS

The observations described were conducted over a wide range of Galactic latitudes and therefore there is a potential for galactic contamination, especially at low latitudes (Bennett et al. 1996; Davies et al. 1996). Galactic synchrotron emission can be up to 75% polarized (Rybicki & Lightman 1979). No maps of polarized synchrotron emission exist at 30 GHz, and extrapolation of measurements at lower frequencies, *e.g.* Brouw & Spoelstra (1976), is not a reliable probe of synchrotron polarization at 30 GHz due to Faraday rotation. Although the unpolarized intensity is not necessarily correlated with the polarized intensity, we limit our susceptibility to polarized synchrotron emission by only using data corresponding to Galactic latitudes $|b| > 25°$, *i.e.* regions of low unpolarized intensity. For reference, extrapolation of the 408 MHz Haslam map assuming 10% polarization over our observing region with $b > 25°$ yields an RMS of only a couple of μK. This is consistent with our null result described below, indicating that we see no evidence of foreground contamination.

6. LIKELIHOOD ANALYSIS FOR POLARIZED CMB FLUCTUATIONS

A Bayesian maximum likelihood analysis with a uniform prior is used to test for polarized fluctuations. Since both Q and U are measured simultaneously, we obtain joint likelihoods for E and B in a model independent fashion (Zaldarriaga 1998). The data from the three frequency channels are combined into a single map for each Stokes parameter using the minimum variance map-making procedure which includes all noise correlations. We form a $2N_{\rm pix}$ element data vector $\mathbf{x}_i \equiv (Q_i, U_i)$ where $i = \{1 \ldots N_{pix}\}$. The likelihood of the model given the data is $L \propto \exp(-\mathbf{x}^T\mathbf{C}^{-1}\mathbf{x}/2)/|\mathbf{C}|^{1/2}$. The covariance matrix $\mathbf{C}_{ij} = \mathbf{S_{ij}} + \mathbf{N_{ij}}$, where $\mathbf{N_{ij}} = \langle \mathbf{x_i^T x_j} \rangle$ is the noise covariance matrix which encodes correlations for both Stokes parameters, at each pixel. The noise covariance matrix also accounts for the offset removal required to combine maps made over long timescales. $\mathbf{N_{ij}}$ is a $2N_{\rm pix} \times 2N_{\rm pix}$ symmetric matrix, with $N_{\rm pix} = 84$ pixels of width 2° for the $|b| > 25°$ Galactic latitude-cut data used for the CMB analysis. $\mathbf{S_{ij}}$ is the signal covariance matrix constructed from a simple flat band power model parametrized by T_E, T_B. To place limits on the polarization we consider spectra for both E and B of the form $\ell(\ell+1)C_\ell^X/2\pi = T_X^2$ with $X \in \{E, B\}$. The Q and U signal correlations are computed by transforming the data coordinate basis to a local basis for each pair of pixels. The local basis exploits the intrinsic symmetries of the Stokes parameter correlation functions (Zaldarriaga 1998; Kamionkowski, Kosowsky, & Stebbins 1997). For each pixel pair the Stokes parameters in the global basis are rotated such that the axis defining the positive Q direction of each pixel lies along the great-circle connecting the pixels. The theory covariance matrix for all pairs of Stokes parameters depends only on the sky

coverage and the underlying E and B-mode power spectra:

$$\mathbf{S_{ij}} = \langle \mathbf{x_i x_j} \rangle = \mathbf{R}(\alpha_{\mathbf{ij}})\mathbf{M}(\widehat{\mathbf{r}}_\mathbf{i} \cdot \widehat{\mathbf{r}}_\mathbf{j})\mathbf{R}(\alpha_{\mathbf{ji}})^\mathbf{T}. \quad (2)$$

Here $\mathbf{M}$ is the covariance matrix using a (Q,U)-convention where the reference direction is the great circle connecting the two points, and $\mathbf{R}(\alpha)$ are the rotation matrices defined by $\mathbf{R}(\alpha) \equiv \begin{pmatrix} \cos 2\alpha & \sin 2\alpha \\ -\sin 2\alpha & \cos 2\alpha \end{pmatrix}$ which rotate the Stokes parameters of the i^{th} pixel into a global reference frame where the reference directions are meridians (Tegmark & de Oliveira-Costa 2000). $\mathbf{S_{ij}}$ is constructed from the individual 2×2 blocks of equation (2) by looping over all pixel pairs, which requires $N_{\rm pix}(N_{\rm pix}+1)/2$ operations. The $\mathbf{M}$-matrix is given by (Zaldarriaga 1998)

$$\mathbf{M}(\widehat{\mathbf{r}}_i \cdot \widehat{\mathbf{r}}_j) \equiv \begin{pmatrix} \langle Q_i Q_j \rangle & 0 \\ 0 & \langle U_i U_j \rangle \end{pmatrix}, \quad (3)$$

where

$$\langle Q_i Q_j \rangle \equiv \sum_\ell \left(\frac{2\ell+1}{4\pi}\right) B_\ell^2 \left[F_{1,\ell}^2(z) C_\ell^E - F_{2,\ell}^2(z) C_\ell^B\right] \quad (4)$$

$$\langle U_i U_j \rangle \equiv \sum_\ell \left(\frac{2\ell+1}{4\pi}\right) B_\ell^2 \left[F_{1,\ell}^2(z) C_\ell^B - F_{2,\ell}^2(z) C_\ell^E\right] \quad (5)$$

$z = \widehat{\mathbf{r}}_i \cdot \widehat{\mathbf{r}}_j$ is the cosine of the angle between the two pixels under consideration, $B_\ell = \exp[-\ell(\ell+1)\sigma_B^2/2]$, σ_B is the beam dispersion $= 0.425\times$ FWHM, and F_1, F_2 are functions of Legendre polynomials as defined in Zaldarriaga (1998) and Tegmark & de Oliveira-Costa (2000). For each point in the $T_E - T_B$ plane, equations 4 and 5 are evaluated and substituted into equations 3 and 2 to compute $\mathbf{S_{ij}}$. The joint likelihood for $\{T_E, T_B\}$ is shown in Figure 2. The 95% confidence limits are obtained by integrating the likelihood function to determine the region which contains 95% of the probability. The limits are $T_E < 10\mu$K and $T_B < 10\mu$K at 95% confidence for the multipole range $2 < \ell < 20$. These limits do not include the ($\sim 10\%$) calibration uncertainty. Also shown in figure 2 are the corresponding limits obtained from our null channels; the QPC. Finally, since the B-mode power is expected to be subdominant, even at large angular scales with no reionization, we have also calculated the limits on T_E with $T_B \equiv 0$. Integrating the 1-D likelihood curve for T_E with $T_B \equiv 0$ we find $T_E < 8\mu$K at 95% confidence.

7. DISCUSSION

POLAR probes the power spectra at large angular scales $2 < \ell < 20$ where the signature of reionization and gravitational waves are predicted to be most pronounced. While we find no evidence for detection of either phenomenon, POLAR'S limits are the most restrictive upper limits at these angular scales, and represent the first limits on E and B-modes from an experiment simultaneously measuring both Q and U. In January 2001 POLAR was upgraded to measure CMB polarization at $20'$ scales. The upgrade, called COsmic Microwave Polarization at Small Scales (COMPASS), uses the same polarimeter as POLAR and is an exciting complement to the results presented here. Assuming similar per-pixel sensitivity to POLAR and a generic E-mode polarization spectrum, COMPASS has the potential to detect polarization of the CMB and dramatically enhance the scientific returns of this nascent field.

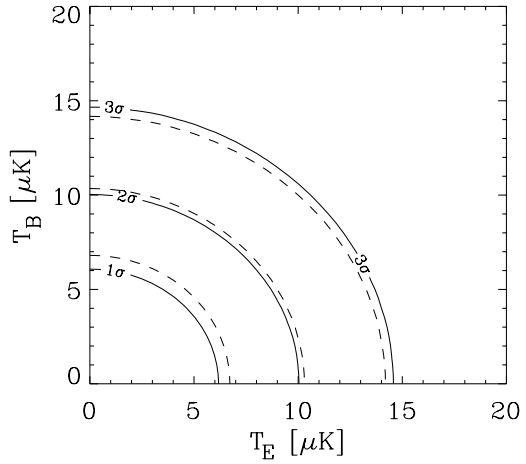

FIG. 2.— Normalized likelihood contour plots in the $T_E - T_B$ plane. The countours enclose are 68%, 95.4%, and 99.7% of the total probability, corresponding to $1, 2$, and 3 standard deviation intervals, as labeled. The solid lines correspond to the joint likelihood for the combined three frequency channels, and the dashed lines are the corresponding null-channel (QPC) likelihood.

We are grateful to Dick Bond, Robert Brandenberger, Brendan Crill, Robert Crittenden, Khurram Farooqui, Josh Gundersen, Wayne Hu, Kip Hyatt, Lloyd Knox, Arthur Kosowsky, Andrew Lange, Phil Lubin, Melvin Phua, Alex Polnarev, Dan Swetz, David Wilkinson, Grant Wilson, Ed Wollack, and Matias Zaldarriaga for many useful conversations. BK and CO were supported by NASA GSRP Fellowships. POLAR'S HEMT amplifiers were graciously provided by John Carlstrom. This work has been supported by NSF grants AST 93-18727, AST 98-02851, and AST 00-71213, and NASA grant NAG5-9194.

REFERENCES

Bennett, C. L., et al. 1996, ApJ, 464, L1
Bond, J. R., Jaffe, A. H., & Knox, L. 1998 , Phys. Rev. D57, 2117
Brouw, W. N., & Spoelstra, T.A. 1976, A&AS, 26, 129
Carretti, E., et al. 2001, New Astronomy, 6, 173
Chandrasekhar, S. 1960, Radiative Transfer, Dover, New York
Davies, R. D., et al. 1996, MNRAS, 278, 883.
Gunn, J. E.. & Peterson, B. A. 1965, ApJ, 142, 1633
Hu, W., and White, M. 1997, New Astron., 2, 323
Kamionkowski, M., Kosowsky, A., and Stebbins, A. 1997, Phys. Rev. D, 55, 7368
Keating, B., Polnarev, A., Steinberger, J., & Timbie, P. 1998, ApJ, 495, 580
Keating, B. 2000, Ph. D. Thesis, Brown University, Providence, RI
Kraus, J. 1982 Radio Astronomy, McGraw-Hill,New York
Lubin, P., & Smoot, G. 1981, ApJ, 245, 1 L51
Nanos, G. 1979, ApJ, 232, 341
Pospisszalski, M. 1992, IEEE MTT-S Digest,1369
Rybicki, G. B.,& Lightman, A. 1979, Radiative Processes in Astrophysics, (New York:Wiley)
Seljak, U., & Zaldarriaga,M. 1996a, ApJ, 469, 437
Tegmark, M. 1997,Phys. Rev. D, 56, 4514
Tegmark, M., and de Oliverira-Costa, A. 2000, astro-ph/0012120
Wang, X., Tegmark, M. & Zaldarriaga, M. 2001, astro-ph/0105091
Wollack, E.J., et al., 1993, ApJ, 419, L49
Wollack, E.J., and Pospieszalski, M., 1998, IEEE MTT-S Digest, 669
Zaldarriaga, M., & Seljak, U. 1997, Phys. Rev. D, 55,1830
Zaldarriaga, M., Spergel,D., Seljak, U 1997 ApJ,488,1
Zaldarriaga, M. 1998, ApJ, 503, 1